15. Eu, J. P., Liu, L., Zeng, M. & Stamler, J. S. An apoptotic model for nitrosative stress. *Biochemistry* **39**, 1040–1047 (2000).

16. Akaike, T. *et al.* Nanomolar quantification and identification of various nitrosothiols by high performance liquid chromatography coupled with flow reactors of metals and Griess reagent. *J. Biochem. (Tokyo)* **122**, 459–466 (1997).

17. Liu, L., Zeng, M., Hausladen, A., Heitman, J. & Stamler, J. S. Protection from nitrosative stress by yeast flavohemoglobin. *Proc. Natl Acad. Sci. USA* **97**, 4672–4676 (2000).

18. Wehner, E. P., Rao, E. & Brendel, M. Molecular structure and genetic regulation of SFA, a gene responsible for resistance to formaldehyde in *Saccharomyces cerevisiae*, and characterization of its protein product. *Mol. Gen. Genet.* **237**, 351–358 (1993).

19. Gutheil, W. G., Holmquist, B. & Vallee, B. L. Purification, characterization, and partial sequence of the glutathione-dependent formaldehyde dehydrogenase from *Escherichia coli*: a class III alcohol dehydrogenase. *Biochemistry* **31**, 475–481 (1992).

20. Shafqat, J. *et al.* Pea formaldehyde-active class III alcohol dehydrogenase: common derivation of the plant and animal forms but not of the corresponding ethanol-active forms (classes I and P). *Proc. Natl Acad. Sci. USA* **93**, 5595–5599 (1996).

21. Uotila, L. & Koivusalo, M. in *Coenzymes and Cofactors* (ed. Dolphin, D.) 517–551 (John Wiley & Sons, New York, 1989).

22. Barber, R. D. & Donohue, T. J. Function of a glutathione-dependent formaldehyde dehydrogenase in *Rhodobacter sphaeroides* formaldehyde oxidation and assimilation. *Biochemistry* **37**, 530–537 (1998).

23. Ras, J. *et al.* Isolation, sequencing, and mutagenesis of the gene encoding NAD- and glutathione-dependent formaldehyde dehydrogenase (GD-FALDH) from *Paracoccus denitrificans*, in which GD-FALDH is essential for methylotrophic growth. *J. Bacteriol.* **177**, 247–251 (1995).

24. Shen, S., Sulter, G., Jeffries, T. W. & Cregg, J. M. A strong nitrogen source-regulated promoter for controlled expression of foreign genes in the yeast *Pichia pastoris*. *Gene* **216**, 93–102 (1998).

25. Kuwada, M., Horie, S. & Ogura, Y. Studies on the Enzymatic reduction of C-nitroso compounds. II. Multiple forms of liver C-nitrosoreductase and the identity with alcohol dehydrogenase. *J. Biochem. (Tokyo)* **88**, 859–69 (1980).

26. Kluge, I., Gutteck-Amsler, U., Zollinger, M. & Do, K. Q. S-nitrosoglutathione in rat cerebellum: identification and quantification by liquid chromatography-mass spectrometry. *J. Neurochem.* **69**, 2599–2607 (1997).

27. Minning, D. M. *et al.* Ascaris haemoglobin is a nitric oxide-activated 'deoxygenase'. *Nature* **401**, 497–502 (1999).

28. Ribeiro, J. M., Hazzard, J. M., Nussenzveig, R. H., Champagne, D. E. & Walker, F. A. Reversible binding of nitric oxide by a salivary heme protein from a bloodsucking insect. *Science* **260**, 539–541 (1993).

29. Glover, R. E., Koshkin, V., Dunford, H. B. & Mason, R. P. The reaction rates of NO with horseradish peroxidase compounds I and II. *Nitric Oxide* **3**, 439–444 (1999).

30. Liu, L., Zeng, M. & Stamler, J. S. Hemoglobin induction in mouse macrophages. *Proc. Natl Acad. Sci. USA* **96**, 6643–6647 (1999).

Covalent inhibition revealed by the crystal structure of the caspase-8/p35 complex

Guozhou Xu*, Maurizio Cirilli*†, Yihua Huang‡, Rebecca L. Rich§, David G. Myszka§ & Hao Wu*

* *Department of Biochemistry, Weill Medical College of Cornell University and* ‡*Program in Physiology, Biophysics and Molecular Medicine, Graduate School of Medical Sciences of Cornell University, 1300 York Avenue, New York, New York 10021, USA*
† *Istituto di Strutturistica Chimica 'Giordano Giacomello', C.N.R., C. P. 10, Monterotondo Stazione, Italy*
§ *Center for Biomolecular Interaction Analysis, School of Medicine, University of Utah, Salt Lake City, Utah 84132, USA*

Apoptosis is a highly regulated process that is crucial for normal development and homeostasis of multicellular organisms[1,2]. The p35 protein from baculoviruses effectively prevents apoptosis by its broad-spectrum caspase inhibition[3–7]. Here we report the crystal structure of p35 in complex with human caspase-8 at 3.0 Å resolution, and biochemical and mutagenesis studies based on the structural information. The structure reveals that the

caspase is inhibited in the active site through a covalent thioester linkage to p35, which we confirmed by gel electrophoresis, hydroxylamine treatment and mass spectrometry experiments. The p35 protein undergoes dramatic conformational changes on cleavage by the caspase. The repositioning of the amino terminus of p35 into the active site of the caspase eliminates solvent accessibility of the catalytic dyad. This may be crucial for preventing hydrolysis of the thioester intermediate, which is supported by the abrogation of inhibitory activity through mutations at the N terminus of p35. The p35 protein also makes conserved contacts with the caspase outside the active-site region, providing the molecular basis for the broad-spectrum inhibitory activity of this protein. We demonstrate a new molecular mechanism of caspase inhibition, as well as protease inhibition in general.

The p35 protein shows unparalleled effectiveness as a broad-spectrum caspase inhibitor against all three groups of caspases from mammals and other metazoans[3–6]. Numerous cellular and *in vivo* studies have implicated the function of p35 in rescuing cells from apoptosis to revive their normal cellular functions[7–12], thereby
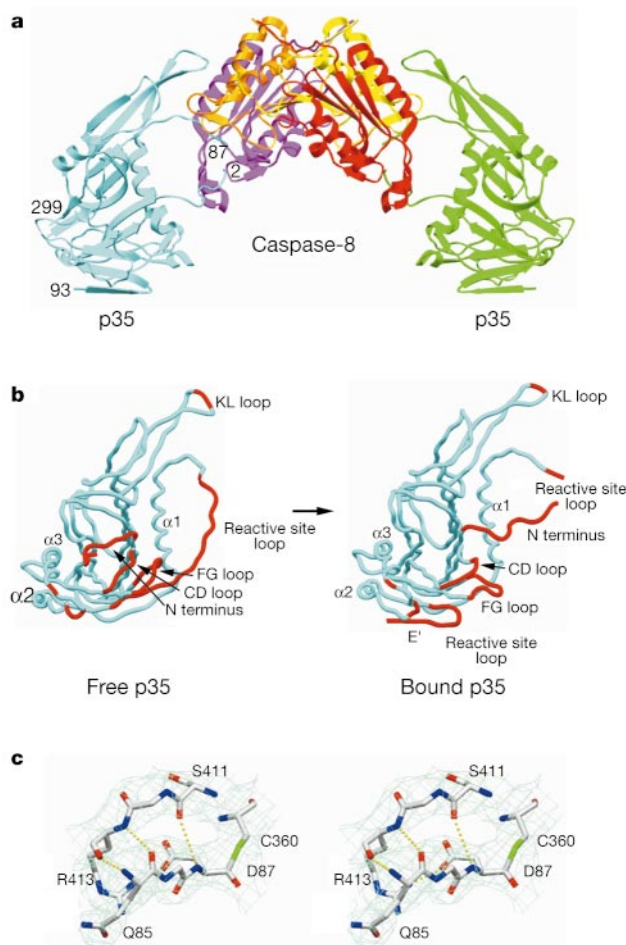
Figure 1 Structure of the p35/caspase-8 complex. **a**, Ribbon diagram of dimeric complex with the two-fold axis in the vertical orientation. p35, cyan and green; α-subunit (p18) of caspase-8, magenta and red; β-subunit (p12) of caspase-8, orange and yellow. Ordered termini for p35-N (residues 2–87) and p35-C (residues 93–299) are labelled. **b**, Conformational transitions of p35 on cleavage. Residues with differences in Cα positions larger than 4.0 Å are shown in red, which include the N terminus (residues 2–12), the CD loop (residues 35–40), the caspase recognition sequence (residues 85–87), the reactive-site loop after the cleavage site (residues 93–101), the FG loop (residues 157–165) and the KL loop (residues 254–255). **c**, Atomic model of the complex near the active site of caspase-8 overlaid with an omit electron density map (1.0σ contour). Potential hydrogen bonds are indicated by dotted lines. Side chains for residue Met 86 of p35 and Tyr 412 of caspase-8 are omitted for clarity.

establishing the basis for its potential in anti-apoptosis therapies. Biochemical characterization has shown that caspase inhibition by p35 correlates with the cleavage of its reactive-site loop at Asp 87 and the formation of a tight complex with the caspase[4,6], by means of an unknown mechanism. To elucidate the molecular basis of p35 function, we determined the crystal structure of the complex between p35 and caspase-8, a group-III-initiating caspase important in apoptosis mediated by tumour necrosis factor (TNF) and Fas (Table 1 and Fig. 1a, b).

Unexpectedly, the electron density map reveals a covalent thioester linkage between the catalytic Cys 360 of caspase-8 and Asp 87 of the bound p35 (Fig. 1c). This is surprising as previous biochemical studies, such as SDS–polyacrylamide gel electrophoresis (SDS–PAGE) experiments, did not observe evidence for a covalent complex between p35 and caspases (refs 6, 13, 14, and data not shown). The crystallographic observation prompted us to re-examine the biochemical experiments. We suspected that the instability of the thioester bond to denaturation treatment might be the reason for the failure to observe this covalent complex on SDS–PAGE. We therefore checked the effects of pH, reducing agent and heat on the integrity of this complex. We found that the complex is destroyed by the heat treatment (100 °C for 3 min) normally recommended for SDS–PAGE[15], irrespective of pH or reducing agent. Under milder heat treatment (80 °C for 2 min), however, the complex exhibits a distinct dependence on reducing agent and pH (Fig. 2a), which is consistent with the stability and chemistry of a thioester bond

Figure 2 Biochemical characterization of the p35/caspase-8 complex. **a**, SDS–PAGE of the complex treated with SDS sample buffers at different pH levels and with or without the reducing agent β-mercaptoethanol (βME). **b**, Gel-filtration profiles of the complexes, treated either with 1.2 M hydroxylamine or 1.2 M NaCl for 2 h at 37 °C, showing the dissociation of p35 on hydroxylamine treatment. For clarity, only the bands for p35-C are shown. **c**, Observed MALDI-TOF mass spectrometry spectrum of the complex. P35-N, residues 2−87; p35-C, residues 88−299. The observed and calculated (in parentheses) molecular masses for each peak are shown. The values on the y axis are arbitrary units. Asterisk, truncated peak.

Table 1 Refinement statistics

Resolution	40–3.0 Å
R_{sym}: overall (last shell)	9.5% (28.9%)
Coverage: overall (last shell)	94.9% (81.7%)
R (free R)	23.6% (29.6%)
Number of reflections used	36,808
Number of protein residues	1,070
Number of protein atoms	8,696
Number of solvent atoms	26

$R_{sym} = \Sigma_h \Sigma_i |I_{hi} - \langle I_h \rangle| / \Sigma_h \Sigma_i I_{hi}$.

between p35 and the caspase[16]. Additional experimental corroboration of the presence of the covalent thioester bond was obtained from the sensitivity of the complex to treatment by hydroxylamine (Fig. 2b), a strong nucleophile often used to break ester bonds[16,17].

The covalent nature of the interaction between p35 and caspases was further confirmed by matrix-assisted laser desorption ionization time-of-flight (MALDI-TOF) mass spectrometry (Fig. 2c), which rarely preserves non-covalent interactions. The observed spectrum of the p35/caspase-8 complex contains a prominent peak at around a relative molecular mass of 28,000 (M_r 28K) that can only be explained by a covalently linked N-terminal fragment of p35 (p35-N, residues 2–87) and the α-subunit of caspase-8 (p18). Consistent with this interpretation, observed peaks for the two individual components (p35-N and p18) are very weak. Furthermore, acid denaturation of the complex in the presence of reducing agent eliminated the 28K peak and enhanced the peaks for the individual components (p35-N and p18). The MALDI-TOF spectrum of the complex of p35 with caspase-3, a group-II-executing caspase, contains a similar peak of high molecular mass, which suggests the generality of the covalent interaction of p35 with caspases.

The trapping of the thioester intermediate between p35 and caspases raises the question as to how the intermediate is stabilized rather than hydrolysed by the enzyme. The structure of the complex suggests that the N terminus of p35 may have a specific and crucial function in this regard by direct blockade of hydrolysis. During normal catalysis, the thioester intermediate is quickly hydrolysed by an activated water molecule bound to the His residue in the catalytic dyad[18]. In the complex, the N terminus of p35 repositions into the active site of caspase-8 from a partially buried conformation in the non-cleaved p35 (Figs 1b and 3a). The interaction eliminates completely solvent accessibility of the critical His 317 residue in caspase-8, which is semi-exposed in the absence of the interaction. Although the resolution of the structure does not permit a definitive assignment, the thiol of Cys 2 also seems to form a hydrogen bond with the imidazole ring of His 317, which distorts His 317 away from an optimal orientation for catalysis. Residue Cys 2—which we demonstrated by mass spectrometry of tryptic peptides to be capped by acetylation—and residue Val 3 make van der Waals contacts with caspase-8, at residues Ile 257, Asp 363 and Tyr 365 (Fig. 3a). The interaction does not seem to affect otherwise the intrinsic catalytic machinery of caspase-8, as the p35/caspase-8 structure superimposes well with other known caspase-8 structures[19,20].

Table 2 Characterization of the interaction between p35 and caspases

p35	Complex formation*	Cleavage*	Interaction with caspase-3 (C163A)†
Wild type	+	+	$K_d = 1.16 \pm 0.01 \times 10^{-7}$ M
C2G	−	+	
V3G	−	+	
Δ2-5	−	+	
Y82A	−	+	$K_d = 3.4 \pm 0.1 \times 10^{-5}$ M

K_d, dissociation constant.
* Complex formation and cleavage by both caspase-3 and caspase-8 were determined by pull-down of caspases using His-tagged p35 proteins.
† Determined by biosensor measurement (see Supplementary Information).
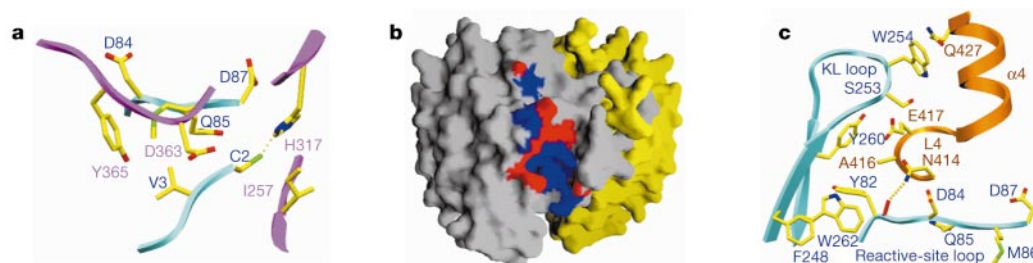
Figure 3 Detailed interaction between p35 and caspase-8. **a**, Interaction near the N terminus of p35 with the active site of caspase-8. p35, cyan; α-subunit of caspase-8, magenta. **b**, Footprint of p35 on the surface of caspase-8 (grey and yellow for each of the αβ-units). Residues conserved among different caspases and main-chain atoms are shown in blue, whereas those with significant variations are shown in red. **c**, Interaction near the KL loop of p35. p35, cyan; β-subunit of caspase-8, orange.

The importance of the N terminus of p35 in the inhibitory mechanism was confirmed by mutagenesis experiments. We created two point mutants (C2G and V3G) and a deletion mutant (Δ2–5) at the N terminus. None of the mutants could form stable complexes with either caspase-8 or caspase-3, based on His-tag pull-down experiments (Table 2). However, all three mutants can be cleaved by both caspases. The C2G mutant is an efficient caspase substrate and exhibits identical behaviour to that of wild-type p35 in expression, solubility and gel-filtration profile. Therefore, the mutational effect of C2G can be attributed to a direct deletion of the important interaction in the complex rather than through significant perturbation of the structure of p35. The V3G and Δ2–5 mutants were cleaved efficiently by caspase-3, but less efficiently by caspase-8. Our gel-filtration experiments showed that they are predominantly dimeric in solution, which is in contrast to monomers for wild-type p35 and the C2G mutant.

Structural analysis of the p35/caspase-8 complex shows that the binding of the p35 N terminus into the active site of the caspase is made possible by the cascade of conformational changes in p35 on its cleavage (Fig. 1b). In the free p35 structure, there is a sequential packing interaction from the reactive-site loop to the FG loop, the CD loop and the N-terminal segment. The pinching of the reactive-site loop in the bound p35 structure suggests that this loop may be highly strained in the initial encounter with the caspase. Therefore, residues after the cleavage site may immediately spring away from the caspase on cleavage. This should instantly cause the sequential relaxation of the FG loop and the CD loop and the release of the N terminus from the core p35 structure to reposition into the active site of the caspase. Side chains adjacent to the N terminus, such as those in helices α2 and α3, move in to fill part of the vacated space. The portion of the reactive-site loop after the cleavage site folds into an extra β-strand (denoted E′) next to the E strand at the edge of the p35 β-sandwich.

These structural transitions in caspase inhibition by p35 explain previous kinetic measurements on the characteristic slow-binding inhibition of p35 (ref. 6) in which the initial encounter is followed presumably by a slower isomerization step. The time scale of the conformational changes must be such that thioester hydrolysis does not occur in the interim between the departure of the P′ residues and the binding of the N terminus into the active site. These two processes are probably highly cooperative, as the strain in the reactive-site loop may pull the P′ residues away as soon as cleavage occurs to allow repositioning of the N terminus into the active site. However, there may be some degree of leakage in the mechanism. This is supported by the apparent deviation from a 1:1 stoichiometry of p35 inhibition for some caspases and the possible turn-overs of p35 by a substrate pathway[6].

The non-covalent interaction between p35 and caspase-8 centres on and extends beyond the tetrapeptide caspase recognition sequence (P4-D[84]QMD[87]-P1) in the reactive-site loop. The contact surface shows significant conservation among different caspases (Fig. 3b), providing an explanation for the wide-spectrum effectiveness of p35 as a caspase inhibitor. The total interaction buries approximately 950 Å^2 of surface area on each partner of the binding interface. The P4–P1 residues are recognized similarly by the S4–S1 sites, as seen in crystal structures of caspases in complex with various peptide inhibitors[19,20], involving specific main-chain and side-chain hydrogen bonds with conserved caspase residues such as Arg 260, Ser 411 and Arg 413. The N terminus of p35 contacts the caspase adjacent to one side of this interaction (Fig. 3a). To the other side, the P6 residue Tyr 82, residues in the K and L strands, and the KL loop interact with residues 414–427 of caspase-8 at the structurally conserved L4 loop and the α4 helix (Fig. 3c). These caspase residues show a lesser degree of conservation at the sequence level, but significant main-chain contacts are used. It is probable that the observed flexibility in the KL loop and the possible flexibility of the N terminus of p35 can accommodate some degree of sequence variation to preserve the interaction.

As the mechanism of caspase inhibition by p35 involves integration of multiple sequence segments, the integrity of the p35 structure is crucial for its function as a caspase inhibitor. Our structure-based alanine mutagenesis for p35 interface residues showed that Tyr 82 at the base of the reactive-site loop is essential for complex formation with caspase-3 and caspase-8, without affecting cleavage. The strength of the initial encountering interaction is also greatly diminished, as assessed by the biosensor measurement of the interaction between p35 and an active site mutant of caspase-3 (C163A), which was processed to its mature form by caspase-8 (Table 2). Tyr 82 helps to glue together the reactive-site loop and the neighbouring KL strands and loop. Its mutation may therefore uncouple these interaction elements for caspases. Disruptive mutations at residues such as Ile 67 and Val 71 have shown similar phenotypes and seem to act by affecting the interaction between the β-sheet core of p35 and the helix (α1) preceding the reactive-site loop[14]. Many reported Ala-Ser insertions and alanine mutagenesis of charged residues in p35 may also be explained by structural perturbations[14,21].

The molecular mechanism of caspase inhibition by p35 reported here is highly distinct from the collection of modes of protease inhibition observed in numerous protease-inhibitor complexes[22]. Most of these protease inhibitors block the active sites of their target proteases either directly or indirectly through extensive non-covalent interactions. Covalent suicide inhibition through ester-bond formation has long been known for serpins, a family of serine protease inhibitors[23], but with a different underlying mechanism. The recent crystal structure of a serpin/protease complex shows distortion of the active site and deformation of the protease by a pulling force from the serpin[24]. In contrast, p35 directly blocks thioester hydrolysis after post-cleavage conformational changes through solvent exclusion and perhaps reorientation of the catalytic residue, providing yet another new mode of protease inhibition. □

Methods

Protein expression and purification

Baculovirus p35 (residues 1–299, with and without a C-terminal His-tag), human caspase-8 (residues S201–D463, with and without a C-terminal His-tag), human caspase-3 (residues 1–277, with and without a C-terminal His-tag) and human caspase-3 active site mutant (C163A; residues 1–277, with a C-terminal His-tag) were expressed in the pET bacterial expression system using isopropylthiogalactoside induction overnight at 20 °C. The His-tagged proteins were purified by Ni-affinity chromatography and gel filtration. Both caspase-8 and caspase-3 were automatically converted to their mature forms during the protein expression and purification procedures. To obtain the p35/caspase-8 complex, the cell pellets of His-tagged caspase-8 were mixed with those containing excess non-tagged p35, and the complex was co-purified using the His-tag in the caspase-8 construct. To generate the mature form of the mutant caspase-3 (C163A), the cell pellets of His-tagged C163A mutant were mixed with those of non-tagged caspase-8. The mixed cells were lysed by repeated bursts of sonication and incubated for 30 min at 37 °C to allow the processing of the C163A mutant by the active caspase-8 in the lysate. The processed C163A mutant was then purified similarly by Ni-affinity and gel filtration.

Crystallization of the p35/caspase-8 complex

The p35/caspase-8 complex eluted from a Superdex 200 gel-filtration column at a position around 130K, corresponding to a complex containing two molecules of p35 and one dimeric $\alpha_2\beta_2$ caspase-8 (α-subunit-p18 and β-subunit-p12). The gel-filtration buffer contained 20 mM Tris at pH 7.5, 150 mM NaCl and 5 mM dithiothreitol. The protein complex was concentrated to 20–30 mg ml^{-1} and crystallized at 20 °C by hanging-drop vapour diffusion. The crystallization reservoir contained 0–2% PEG8K, 100 mM MOPS at pH 7.5 and 1% 2-propanol. The reduction in salt concentration in the crystallization drop after mixing the complex with the reservoir seems to have been the principal force that decreased the solubility of the complex to allow saturation and crystallization.

Data collection and structural determination

The crystals belong to space group $C222_1$ with cell dimensions $a = 100.0$ Å, $b = 117.3$ Å and $c = 346.5$ Å. Although the crystals looked indistinguishable, more than 95% of the crystals are intrinsically twined. An initial 3.5-Å diffraction data set from a single crystal was collected at the X4A beamline of National Synctrophon Light Source, from which a molecular replacement solution was obtained using the atomic models of free p35 (ref. 13) and the $\alpha\beta$-form of a caspase-8 structure[20] using the program Replace[25]. Each asymmetric unit of the crystals contains two p35 molecules and two separate $\alpha\beta$-units of caspase-8. The two-fold axes of the caspase-8 dimers coincide with the crystallographic axes. A 3.0-Å data set was collected at the Commercial Collaborative Access Team of the advanced photon source for model building[26] and refinement[27]. Marked conformational rearrangements were observed for p35 and built on the basis of $2F_o–F_c$ maps and averaged electron density maps.

Mass spectrometry

MALDI-TOF analyses were performed in the linear positive-ion mode with delayed ion extraction using a Biflex III mass spectrometer (Bruker Daltonik). Desalted samples in 0.1% aqueous trifluoroacetic acid (TFA) were mixed 1/1 (v/v) with a matrix consisting of 10 mg ml^{-1} 2,5-dihydroxybenzoic acid dissolved in acetonitrile/water/TFA (50/50/0.1 (v/v/v)) and spotted on a highly polished stainless target. Spectra were calibrated using the singly and doubly charged peaks of horse skeletal muscle apomyoglobin as either internal or external standards. We collected and analysed spectra using proprietary Bruker software.

Biosensor measurement

The interaction of p35 with the mature form of the active-site mutant of caspase-3 (C163A), which was immobilized on the sensor chip by amine-coupling chemistry, was measured by surface plasmon resonance using a BIACORE 2000. The experiment was performed similarly as described for the interaction between TRAF2 and TRADD[28]. All response data were double referenced[29], thereby correcting for bulk refractive index changes and nonspecific p35 binding to the sample and reference surfaces. Data were fitted globally to a simple interaction model (A + B = AB) using CLAMP[30].

His-tag pull-down assay

Purified His-tagged wild-type or mutant p35 proteins were mixed with cell pellets of non-tagged caspase-8 or caspase-3 and lysed in 50 mM phosphate at pH 8.0, 150 mM NaCl, 10 mM imidazole and 10 mM β-mercaptoethanol. Pre-equilibrated Ni-NTA resins were incubated with the mixtures at 4 °C overnight and washed three times with the same buffer. The bound proteins were eluted with 200 mM imidazole and analysed on SDS–PAGE.

1. Thompson, C. B. Apoptosis in the pathogenesis and treatment of disease. *Science* **267,** 1456–1461 (1995).
2. Steller, H. Mechanisms and genes of cellular suicide. *Science* **267,** 1445–1449 (1995).
3. Clem, R. J., Fechheimer, M. & Miller, L. K. Prevention of apoptosis by a baculovirus gene during infection of insect cells. *Science* **254,** 1388–1390 (1991).
4. Bump, N. J. *et al.* Inhibition of ICE family proteases by baculovirus antiapoptotic protein p35. *Science* **269,** 1885–1888 (1995).
5. Xue, D. & Horvitz, H. R. Inhibition of the *Caenorhabditis elegans* cell-death protease CED-3 by a CED-3 cleavage site in baculovirus p35 protein. *Nature* **377,** 248–251 (1995).
6. Zhou, Q. *et al.* Interaction of the baculovirus anti-apoptotic protein p35 with caspases. Specificity, kinetics, and characterization of the caspase/p35 complex. *Biochemistry* **37,** 10757–10765 (1998).
7. Ekert, P. G., Silke, J. & Vaux, D. L. Caspase inhibitors. *Cell Death Differ.* **6,** 1081–1086 (1999).
8. Hay, B. A., Wolff, T. & Rubin, G. M. Expression of baculovirus P35 prevents cell death in *Drosophila*. *Development* **120,** 2121–2129 (1994).
9. White, K., Tahaoglu, E. & Steller, H. Cell killing by the *Drosophila* gene reaper. *Science* **271,** 805–807 (1996).
10. Beidler, D. R., Tewari, M., Friesen, P. D., Poirier, G. & Dixit, V. M. The baculovirus p35 protein inhibits Fas- and tumor necrosis factor-induced apoptosis. *J. Biol. Chem.* **270,** 16526–16528 (1995).
11. Robertson, N. M. *et al.* Baculovirus P35 inhibits the glucocorticoid-mediated pathway of cell death. *Cancer Res.* **57,** 43–47 (1997).
12. Hisahara, S. *et al.* Targeted expression of baculovirus p35 caspase inhibitor in oligodendrocytes protects mice against autoimmune-mediated demyelination. *EMBO J.* **19,** 341–348 (2000).
13. Fisher, A. J., Cruz, W., Zoog, S. J., Schneider, C. L. & Friesen, P. D. Crystal structure of baculovirus P35: role of a novel reactive site loop in apoptotic caspase inhibition. *EMBO J.* **18,** 2031–2039 (1999).
14. Zoog, S. J., Bertin, J. & Friesen, P. D. Caspase inhibition by baculovirus P35 requires interaction between the reactive site loop and the beta-sheet core. *J. Biol. Chem.* **274,** 25995–26002 (1999).
15. Sambrook, J., Fritsch, E. F. & Maniatis, T. *Molecular Cloning*, 2nd edn (Cold Spring Harbor Laboratory Press, New York, 1989).
16. Bruice, T. C. & Benkovic, S. J. *Bioorganic Mechanisms* (Benjamin, New York, 1966).
17. Owen, W. G., Penick, G. D., Yoder, E. & Poole, B. L. Evidence for an ester bond between thrombin and heparin cofactor. *Thromb. Haemost.* **35,** 87–95 (1976).
18. Stennicke, H. R. & Salvesen, G. S. Catalytic properties of the caspases. *Cell Death Differ.* **6,** 1054–1059 (1999).
19. Watt, W. *et al.* The atomic-resolution structure of human caspase-8, a key activator of apoptosis. *Structure Fold Des.* **7,** 1135–1143 (1999).
20. Blanchard, H. *et al.* The three-dimensional structure of caspase-8: an initiator enzyme in apoptosis. *Structure Fold Des.* **7,** 1125–1133 (1999).
21. Bertin, J. *et al.* Apoptotic suppression by baculovirus P35 involves cleavage by and inhibition of a virus-induced CED-3/ICE-like protease. *J. Virol.* **70,** 6251–6259 (1996).
22. Bode, W. & Huber, R. Structural basis of the endoproteinase–protein inhibitor interaction. *Biochim. Biophys. Acta* **1477,** 241–252 (2000).
23. Wright, H. T. & Scarsdale, J. N. Structural basis for serpin inhibitor activity. *Proteins* **22,** 210–225 (1995).
24. Huntington, J. A., Read, R. J. & Carrell, R. W. Structure of a serpin–protease complex shows inhibition by deformation. *Nature* **407,** 923–926 (2000).
25. Tong, L. REPLACE, a suite of computer programs for molecular-replacement calculations. *J. Appl. Cryst.* **26,** 748–751 (1993).
26. Jones, T. A., Zou, J. -Y., Cowan, S. W. & Kjeldgaard, M. Improved methods for building models in electron density maps and the location of errors in those models. *Acta Crystallogr. A* **47,** 110–119 (1991).
27. Brunger, A. T. *et al.* Crystallography & NMR system: a new software suite for macromolecular structure determination. *Acta Crystallogr. D* **54,** 905–921 (1998).
28. Park, Y. C. *et al.* A novel mechanism of TRAF signaling revealed by structural and functional analyses of the TRADD–TRAF2 interaction. *Cell* **101,** 777–787 (2000).
29. Myszka, D. G. Improving biosensor analysis. *Mol. Recogn.* **12,** 1–6 (1999).
30. Myszka, D. G. & Morton, T. A. CLAMP: a biosensor kinetic data analysis program. *Trends Biochem. Sci.* **23,** 149–150 (1998).

Supplementary information is available on *Nature*'s World-Wide Web site (http://www.nature.com) or as paper copy from the London editorial office of *Nature*.

Correspondence and requests for materials should be addressed to H.W. (e-mail: haowu@med.cornell.edu). Atomic Coordinates are deposited in the Protein DataBank under accession number 1I4E.